Antibacterial Photodynamic Therapy in the Near-Infrared Region with a Targeting Antimicrobial Peptide Connected to a π-Extended Porphyrin

Charly Gourlot, Alexis Gosset, Elise Glattard, Christopher Aisenbrey, Sabarinathan Rangasamy, Morgane Rabineau, Tan-Sothea Ouk, Vincent Sol, Philippe Lavalle, Christophe Gourlaouen, et al.

Antibacterial Photodynamic Therapy in the Near Infrared with a Targeting Antimicrobial Peptide Connected to a π-Extended Porphyrin.

Charly Gourlot,[§] Alexis Gosset,[§] Elise Glattard,[⸸] Christopher Aisenbrey,[⸸] Sabarinathan Rangasamy,[ǂ] Morgane Rabineau,[†] Tan-Sothea Ouk,[‡] Vincent Sol,[‡] Philippe Lavalle,[†] Christophe Gourlaouen,[±] Barbara Ventura,* Burkhard Bechinger,*[⸸] and Valérie Heitz *[§]

[§] Laboratoire de Synthèse des Assemblages Moléculaires Multifonctionnels, Institut de Chimie de Strasbourg, CNRS/UMR 7177, Université de Strasbourg, 4, rue Blaise Pascal, 67000 Strasbourg (France); *E-mail: v.heitz@unistra.fr

[⸸] Biophysique des membranes et RMN, Institut de Chimie de Strasbourg, CNRS/UMR 7177, Université de Strasbourg, 4, rue Blaise Pascal, 67000 Strasbourg (France); *E-mail: bechinge@unistra.fr

[ǂ] Istituto per la Sintesi Organica e la Fotoreattività (ISOF) – Consiglio Nazionale delle Ricerche (CNR), Via P. Gobetti 101, Bologna (Italy); *E-mail: barbara.ventura@isof.cnr.it

[†] Institut National de la Santé et de la Recherche Médicale, INSERM U1121 Biomaterials and Bioengineering, 1 rue Eugène Boeckel, 67000 Strasbourg, France - Université de Strasbourg, Faculté de Chirurgie Dentaire, 8 rue Sainte Elisabeth, 67000 Strasbourg, France

[‡] Université de Limoges, Laboratoire PEIRENE, UR 22722, 123 Avenue Albert Thomas, 87060 Limoges, (France)

[±] Laboratoire de Chimie Quantique, Institut de Chimie de Strasbourg, CNRS/UMR 7177, Université de Strasbourg, 4, rue Blaise Pascal, 67000 Strasbourg (France)

Abstract.

The increase of antimicrobial resistance to conventional antibiotics is worldwide a major health problem that requires the development of new bactericidal strategies. Antimicrobial photodynamic therapy (a-PDT) that generates reactive oxygen species acting on multiple cellular targets is unlikely to induce bacterial resistance. This localized treatment requires, for safe and efficient treatment of non-superficial infections, a targeting photosensitizer excited in the near IR. To this end, a new conjugate consisting of an antimicrobial peptide linked to a π-extended porphyrin photosensitizer was designed for a-PDT. Upon irradiation at 720 nm, the conjugate has shown at micromolar concentration, strong bactericidal action on both Gram-positive and Gram-negative bacteria. Moreover, this conjugate allows to reach a low minimum bactericidal concentration with near IR excitation without inducing toxicity to skin cells.

Keywords: Antimicrobial photodynamic therapy- near infrared – porphyrin - antimicrobial peptide - bacteria - keratinocyte

The worldwide increase of bacterial strains resistant to multiple antibiotics and the emergence of new resistance mechanisms poses a serious threat to public health. Due to the selective pressure exerted on pathogenic microorganisms, multiresistant strains can become predominant when at the same time alternative treatments are missing. Thus, there is an urgent need to develop new drugs or alternative therapeutics to stop the spread of multidrug-resistant bacteria.[1] For such, drugs with a non-specific mode of action, based on the production of reactive oxygen species (ROS) that damage various cell constituents, are attractive. Photodynamic therapy (PDT) that uses the combination of a non-toxic chromophore called photosensitizer (PS), light of appropriate wavelength and oxygen is an efficient process to generate ROS.[2,3] Following light absorption, the excited PS reacts with surrounding oxygen by energy or electron transfer

to generate singlet oxygen and other ROS inducing lethal tissue and vascular damages. PDT is already applied to treat diseases in dermatology, ophthalmology and localized cancerous tumors either as the main treatment or in combination with surgery, radiotherapy and chemotherapy. Moreover, PDT applied to the destruction of pathogen microorganisms, known as antimicrobial photodynamic therapy (a-PDT), was explored as an alternative treatment to antibiotics. It has shown promising results towards bacteria, viruses and fungi by the oxidative damage generated by ROS to cellular constituents such as lipids, proteins, nucleic acids, polysaccharides.[4,5] The strength of a-PDT resides in low propensity of microorganisms to develop resistance to a multi-target treatment and its effectiveness against both sensitive and multi-resistant bacteria.[6] It has the potential to treat a wide variety of local and chronic infections responsible for long-term hospitalizations.[7] PDT has also shown to trigger an immune response making a-PDT well adapted for local wound disinfection.[8] Nevertheless several issues remain to be solved for safe and efficient a-PDT applications to a broad range of pathogens found in infections. Gram-negative bacteria have a peculiar membrane of low permeability that make these pathogens more difficult to kill than Gram-positive bacteria. Neutral or negatively charged organic dyes that photoinactivate Gram-positive bacteria have no or low efficiency on Gram-negative bacteria.[9,10] In contrast, the ones endowed with positive charges disorganize and permeabilize both Gram-positive and Gram-negative membranes leading to their efficient photoinduced inactivation.[11-14] Efficacy strongly depends on the nature of the PS and methylene blue, a phenothiazinium dye, has its photodisinfection activity hampered by its rejection by bacterial efflux pumps.[15] Small cationic PS are also susceptible to passive diffusion in host cells leading to toxicity.

To increase the selectivity of a-PDT towards bacteria over human cells, the use of a targeting unit to selectively drive the PS to bacteria is a promising strategy. Several trials with cationic lysine[16,17] or ethyleneimine-based polymers[18] have improved the activity towards Gram-

negative bacteria. Of interest are antimicrobial peptides (AMP) found in animals, plants, and fungi that have shown selectivity towards bacteria over human cells.[19] Interestingly, porphyrin-AMP conjugates reported with linear[20–24], cyclic[25–28] or with a lipopolysaccharide-binding peptide[29] have shown increased photoinactivation of bacteria as compared to the components used individually. Nevertheless, the selectivity remains an issue since some good photobactericidal results were shattered by toxicity on mammalian cells[21,23,25] whereas in other cases toxicity studies were not reported.

The excitation wavelength of the PS is another important issue. Whereas the PSs tested for a-PDT absorb mainly in the visible range, excitation should be performed within the optical therapeutic window (700-900 nm). These wavelengths are weakly absorbed by endogenous chromophores such as hemoglobin and melanin thus preventing photodamage to healthy tissue while giving enough energy for the PS to generate cytotoxic ROS.[30] They also ensure lower scattering and enough penetration of light for a-PDT treatment at a depth of 4 mm,[31,32] for wound infections that extend to the dermis, periodontal diseases and root canal disinfection.[33] Nevertheless, this low energy range of excitation requires an amphiphilic PS designed to have strong near IR absorption and singlet oxygen generation capacity. Although bacteriochlorins and phthalocyanines have propensity to absorb in the NIR, their drawbacks such as reduced stability and photostability for bacteriochlorins and high hydrophobicity for phthalocyanines must be overcome for a-PDT applications.[3,7,33] Chemical modifications of their structure, in particular with the addition of cationic groups to promote water solubility and electrostatic attraction to the negative bacterial wall have proven in some cases effective for significant photodynamic inactivation of Gram-positive and Gram-negative bacteria, with limited toxicity on host cells.[34-36] Nevertheless, phthalocyanine and bacteriochlorin derivatives associated with bacterial targeting units have not received much attention yet. One of the rare examples is a boronic acid functionalized Si(IV) phthalocyanine with absorption extending in the NIR that

can bind to the polysaccharides of the bacterial cell membrane.[37] Strong reduction in the viability of *E. coli* in planktonic and biofilm cultures was achieved upon irradiation at wavelengths above 610 nm from a polychromic light source. Another strategy for near IR absorption is the use of metal-based nanoparticles consisting of different components that enable by up-conversion or energy transfer processes to generate the PS in the excited state.[7] These nanomaterials have nevertheless limitations regarding their applicability due to their potential toxicity and the difficulty in gauging the drug-dose needed for an optimal therapeutic outcome.

Herein, the design of a photoactivable conjugate that consists of a near IR absorbing PS connected to a bacteria-targeting AMP is reported. The selected peptidyl-glycine-leucine-carboxyamide (PGLa) is a natural linear amphipathic peptide with a wide range of antimicrobial activities, whose interactions with bacterial membranes have been studied.[38–40] As PS, a π-extended porphyrin chromophore was designed to generate ROS following near IR excitation. The nature of the lowest excited state of the PS was revealed through computed molecular frontier orbitals. For the conjugate PS-PGLa, the photophysical properties and singlet oxygen generation were determined. The photoinactivation property following excitation in the near IR was evaluated for Gram-positive and Gram-negative bacteria and compared to the individual PS and PGLa components. Also, to assess the relevance of the photobactericidal effect, the phototoxicity induced on normal skin cells under the same irradiation conditions was evaluated.

RESULT AND DISCUSSION

Design and synthesis

PGLa is produced and stored in the skin of the frog Xenopus *laevis* and was one of the first peptides for which antimicrobial activities with high selectivity were described. This appealing property is attributed to a medium-sized structure of 21 amino acids, a net cationic charge of

four from the protonated lysines (K), a high hydrophobicity value of 0.363[41,42] and a hydrophobic moment of 0.378.[43] PGLa has been characterized extensively by NMR structural and biophysical investigations.[42,44] It accumulates in a selective manner at the negatively charged outer surface of bacteria, where it adopts an amphipathic helical structure. The hydrophobic face of the peptide drives its insertion into the interface of the bacterial membrane.[44] The resulting membrane destabilization and passage into the cellular interior have been shown early on to disrupt the energy metabolism of the bacterial cell.[39,40,45,46] This peptide has also a limited number of amino acids known to be susceptible to ROS oxidation/degradation such as methionine (M).[47] Noteworthy PGLa in presence of magainin 2, an AMP belonging to the same magainin family, has shown a synergistic enhancement of the antibacterial activities.[46,48] This is of interest also in the context of developing targeted PS of high selectivity for a-PDT.

As PSs, we have developed π-extended chromophores based on *meso* 5,15-ethynylporphyrin connected to various chromophore with π-delocalized system.[49] In the present case, the photosensitizer precursor **2** is a *meso* 5,15-ethylnylporphyrin connected respectively to a 2-nitrothiophene and a phenoxy group to provide an extended π-conjugated push-pull system. On the two remaining *meso* positions of the porphyrin, the phenyls decorated with two triethyleneglycol chains confer an amphiphilic character to the PS.

The photosensitizer-peptide conjugate **1** was designed by convergent synthesis from porphyrin precursor **2** and resin-grafted PGLa peptide **3** as shown in Scheme 1.

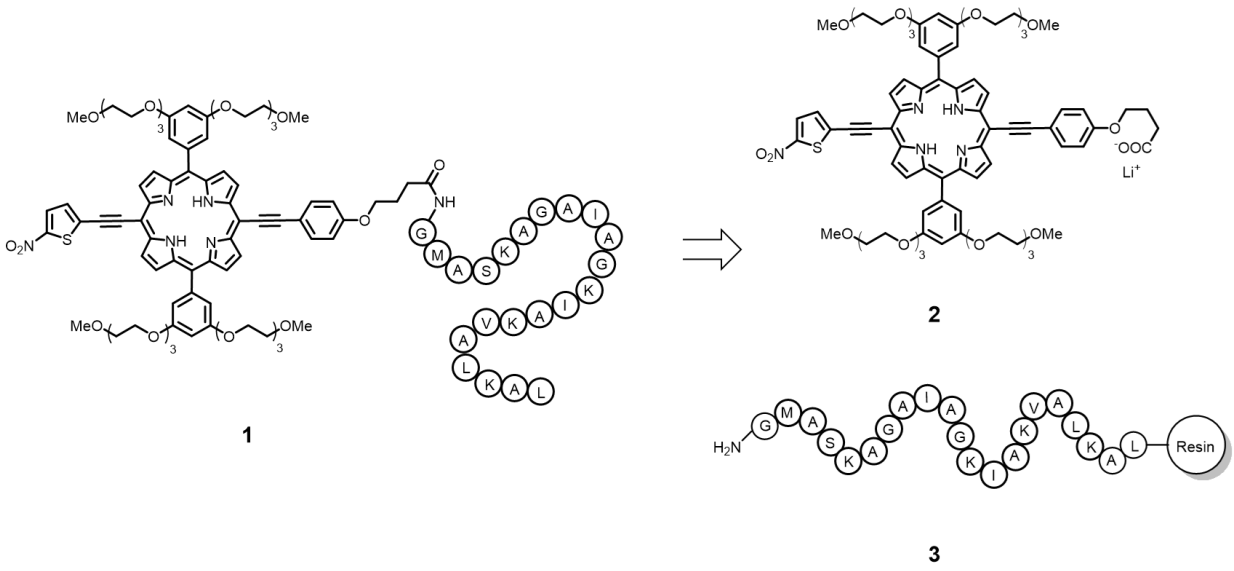

Scheme 1. Retrosynthesis approach used for the targeted porphyrin-PGLa conjugate **1** from the functionalized porphyrin **2** and resin-grafted PGLa peptide **3**.

Conventional solid-phase peptide synthesis using Fmoc chemistry was used to afford amino acid side chains protected-PGLa still grafted on the resin **3**.[50] The PS precursor **2** was obtained starting from the mono-TIPS protected bis-ethynyl porphyrin **4** whose synthesis has been already reported.[49] A short linker to bind the peptide to the porphyrin **2** was introduced with a Sonogashira coupling reaction with the iodo-derivative **5** prepared in one-step from commercial *p*-iodophenol (Scheme 2). The reaction afforded porphyrin **6** in 70% yield. It was engaged, after removal of the TIPS group with TBAF, in a Sonogashira coupling reaction with 1.5 equiv of 2-iodo-5-nitrothiophene **7**. The reaction was performed in THF at 40°C with CuI (10 mol%) and $Pd(PPh_3)_4$ (10 mol%) as catalysts and using $(iPr)_2NH$ as base. After 2 hours, the reaction was completed and 2-nitrothiophene functionalized porphyrin **8** was isolated in 94 % yield following purification by column chromatography. In the next step, Zn(II) porphyrin **8** was demetallated using TFA in dichloromethane (DCM) to afford the free-base porphyrin **9** in almost quantitative yield. Crystals of **9** suitable for X-ray analysis were obtained for this photosensitizer that will be used as a reference of the non-targeted PS. The structure attested

the planarity of the 5,15-bis(acetylene) porphyrin linking nitrothiophene and phenoxy groups (see Supporting Information, Figure S19). Finally, saponification of the ester function of **9** using LiOH gave **2** in 86 % yield.

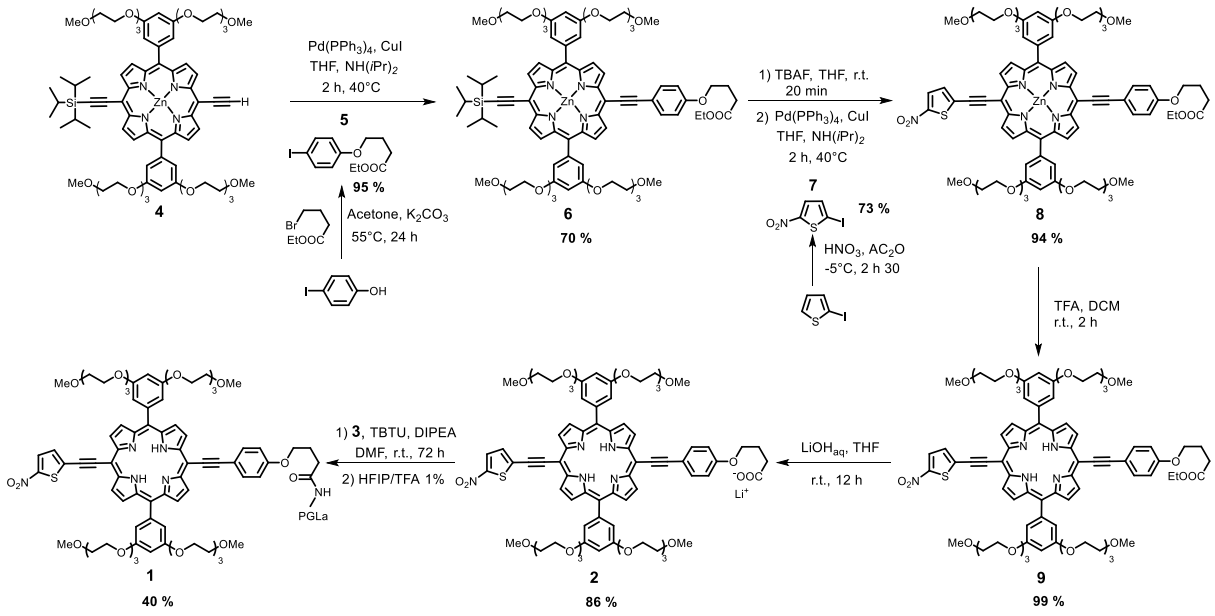

Scheme 2. Synthesis of the porphyrin-peptide conjugate **1**.

The final coupling step was performed using resin-linked PGLa **3** pre-swelled in DMF and the carboxylic acid-functionalized PS **2** which was activated using *O*-(benzotriazol-1-yl)-N,N,N',N'-tetramethyluronium tetrafluoroborate (TBTU) and *N*,*N*-diisopropylethylamine (DIPEA) as a base in DMF. After 72 hours of reaction at room temperature, cleavage of the products from the resin and removal of the protective groups were carried out with a solution of HFIP/TFA (99 : 1). Purification by reversed-phase HPLC afforded the conjugate in greater than 97% purity and 40% yield. High-resolution ESI-MS gave the cationic species $[M + 3 H]^{3+}$ /3 at m/z = 1143.9333 as major species with an isotopic profile in accordance with the theoretical profile at m/z = 1143.9303.

Photophysical and photochemical properties

Absorption and emission properties of compounds **1** and **9** have been determined in DMSO as common solvent, and could be analyzed also in DCM for precursor **9** and in H_2O (pH = 7) for conjugate **1**, due to their proper solubility in these solvents. Figure 1 shows the absorption and emission spectra of **1** and **9** in DMSO (comparison with the spectra recorded in the other solvents is reported in Figure S29).

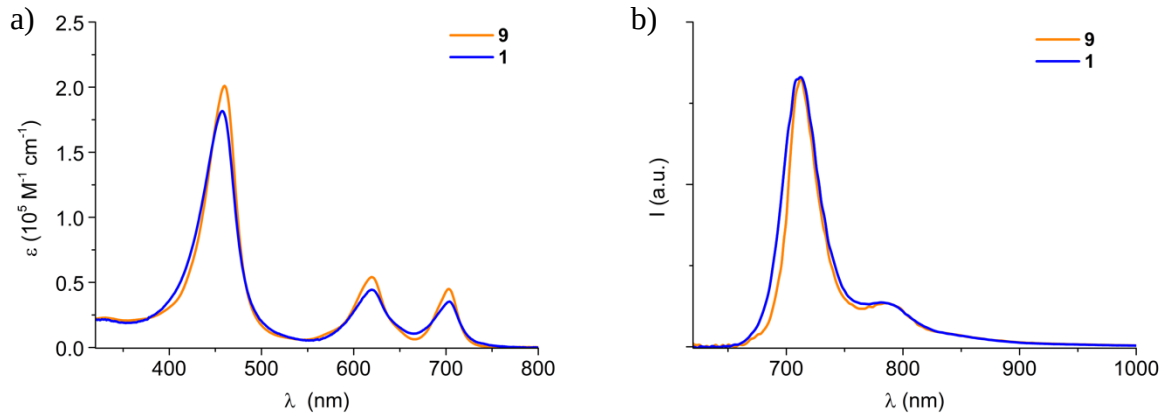

Figure 1. Absorption (a) and normalized corrected emission (b) spectra of **9** and **1** in DMSO (λ_{exc} = 630 nm).

The absorption spectra of porphyrin **9** and conjugate **1** in DMSO present similar features: the absorption is extended up to 750 nm, due to the electronic conjugation of the systems, with two intense Q-bands at ca. 620 nm and 700 nm. The presence of two Q-bands only is quite unusual for free-base porphyrins and can be attributed to charge-transfer transitions involving the 2-nitrothiophene unit which is a strong electron acceptor (as discussed below in the computational section). The absorption spectrum of **9** in DCM shows similar features, while the spectrum of **1** in H_2O appears broadened and red-shifted in the Q-bands region, with absorption tailing at 800 nm (Figure S29).

Emission data for the two compounds are summarized in Table 1. Compounds **9** and **1** show fluorescence in the far red to near IR region, with maximum at 712 nm in DMSO and extension up to 1000 nm (Figure 1b and S29). Porphyrin **9** shows a fluorescence quantum yield of 0.10-0.16, relatively high for a near IR emitting compound, ascribable to the large conjugation of the system,[49,51,52] and an excited state lifetime of the order of 1-2 ns, which is unusually low for a free-base porphyrinic species and can originate from the charge-transfer nature of the emissive singlet state. Conjugate **1** presents a halved fluorescence quantum yield in DMSO and an important decrease in yield in H_2O (Table 1). Interestingly, the emission spectrum of **1** in H_2O appears broad and red-shifted, ranging from 700 to 1200 nm (Figure S29). These features, together with the detection of a multi-exponential fluorescence decay (Table 1), suggests the presence of aggregates (likely J-type) in aqueous solutions of **1**. Comparison of the data of the two compounds in DMSO reveals that the introduction of the peptide is not strongly affecting the emission properties of the photosensitizer, with a slight decrease of the radiative rate constant (from 8.3×10^7 s^{-1} to 4.8×10^7 s^{-1}) and only a minor increase of the non-radiative rate constant (from 7.5×10^8 s^{-1} to 9.5×10^8 s^{-1}, Table 1).

Table 1. Luminescence data at room temperature for **9** and **1** in the different solvents.

		λ_{max} (nm)[a]	ϕ_{fl} [b]	τ (ns) [c]	k_r (s^{-1})	k_{nr} (s^{-1})	ϕ_Δ [d]
9	DMSO	712, 786	0.10	1.2	8.3×10^7	7.5×10^8	0.21
	DCM	708, 782	0.16	2.3	7.0×10^7	3.6×10^8	0.35
1	DMSO	712, 786	0.048	1.0	4.8×10^7	9.5×10^8	0.18
	H_2O	748	1.4×10^{-3}	≤ 0.2 (60%); 1.0 (40%)	2.7×10^6 [e]	1.9×10^9 [e]	≈ 0.10[f]

[a] Emission maxima from corrected spectra. [b] Fluorescence quantum yields measured with reference to DPP-ZnP-DPP in aerated DCM (ϕ_{fl} = 0.16).[49] [c] Excited state lifetimes, excitation at 465 nm (in brackets: fractional intensities); the decays and relative fittings are shown in Figure S30. [d] Singlet oxygen production quantum yields, obtained by direct method in DCM and by indirect method in DMSO and H_2O (see the Supporting Information for details). [e] k_r and

k_{nr} values have been derived by considering a weighted lifetime. [f] Value affected by a large error, see the text for details.

Singlet oxygen quantum yield determinations were performed by direct measurement of singlet oxygen phosphorescence in DCM and D_2O and by indirect methods in DMSO and H_2O (details for both methods are provided in the Supporting Information and Figures S31-S35). Values close to 0.20 are found for both **9** and **1** in DMSO, a solvent where aggregation issues can be excluded. For **1** in H_2O a value of $\phi_\Delta \leq 0.10$ was estimated by a direct method in D_2O (see the experimental section in the Supporting Information and Figure S32), while a value of 0.23 was estimated by means of an indirect method (Figure S35). Since both methods brought some sources of error, we considered a value of ca. 0.10 for the yield of singlet oxygen production of **1** in H_2O (Table 1). The lower value found in water can be ascribed to the presence of aggregates in this solvent but it should be noted that it does not reflect the real ability of the conjugate to generate singlet oxygen once bound to the membrane (see below, in the analysis of association of the conjugate to bacteria). Overall, the results indicate that the presence of the peptide in conjugate **1** is not affecting the singlet oxygen production capacity of precursor **9**, thus rendering it a promising photosensitizer with antimicrobial targeting.

Computed electronic structure of the photosensitizer 9

TD-DFT methods were used to determine the nature of the low energy S1 state of **9**, the PS constituent of the conjugate. Three structures were considered, $\mathbf{C_1}$ with the 2-nitrothiophene, porphyrin and phenoxy group coplanar, $\mathbf{C_2}$ with the phenoxy group perpendicular to the 2-nitrothiophene-porphyrin plane and $\mathbf{C_3}$ with the 2-nitrothiophene perpendicular to the porphyrin-phenoxy plane (Figure 2a). Free rotation of these substituents is expected with a rotational barrier, evaluated in DCM with GAUSSIAN, of 3.2 kcal mol^{-1} for the 2-

nitrothiophene moiety and of 2.3 kcal mol^{-1} for the phenoxy fragment. The geometry of **C_1**, computed with ADF, was obtained after optimization starting from the X-ray structure of **9**. The geometries of **C_2** and **C_3** are that of **C_1** with the phenoxy rotated of 90° for **C_2** or with the 2-nitrothiophene rotated by 90° for **C_3**, both without any re-optimization. The theoretical photophysics was computed with ADF on the basis of these three geometries.

The calculated low energy S_1 absorption bands for the three structures **C_1-C_3** and the experimental absorption spectra of **9** are shown in Figure 2b. The absorption spectra of **C_1** displays an intense peak at 750 nm corresponding to an almost pure (96%) HOMO-LUMO transition. We want to point out that the HOMO-LUMO energy gap (Figure 2c) cannot directly be compared to S_0 to S_1 energy transition (Figure 2b).[53] Similar feature is observed for structure **C_2** associated to a blue shift of the absorption at 701 nm. In **C_3**, the first transition at 707 nm loses all intensity, the intense peak being generated by the second singlet transition at 640 nm, a HOMO-LUMO+1 transition. The blue shift is correlated to a decrease in the conjugation of the porphyrin core to the 2-nitrothiophene and phenoxy substituents leading to an increase in the HOMO-LUMO gap. The nature of the frontier molecular orbitals that contribute to the lowest energy singlet state confirmed the trend observed as shown in Figure 2c.

For the three conformers, the HOMO-LUMO transition that contributes for 90% to the lowest energy band has a strong charge transfer character. The transition involves the delocalized frontier orbitals of the bis-ethynyl porphyrin over the coplanar substituents (HOMO) to the 2-nitrothiophene unit with a contribution of the porphyrin when coplanar (LUMO). The phenoxy electron-donating group conjugated to the porphyrin raises the HOMO of **C_1** by 0.129 eV compared to **C_2**. The strong π-electron acceptor character of the 2-nitrothiophene unit coplanar to the porphyrin in **C_1** stabilizes the LUMO by 0.160 eV as compared to **C_3**. In **C_3**, the absorbing band at 640 nm is due to a π–π* transition centered on the porphyrin core. The low barriers

computed for the rotation of either the 2-nitrothiophene or phenoxy moieties are the source of the shifts of the computed spectra as compared to the experimental one.

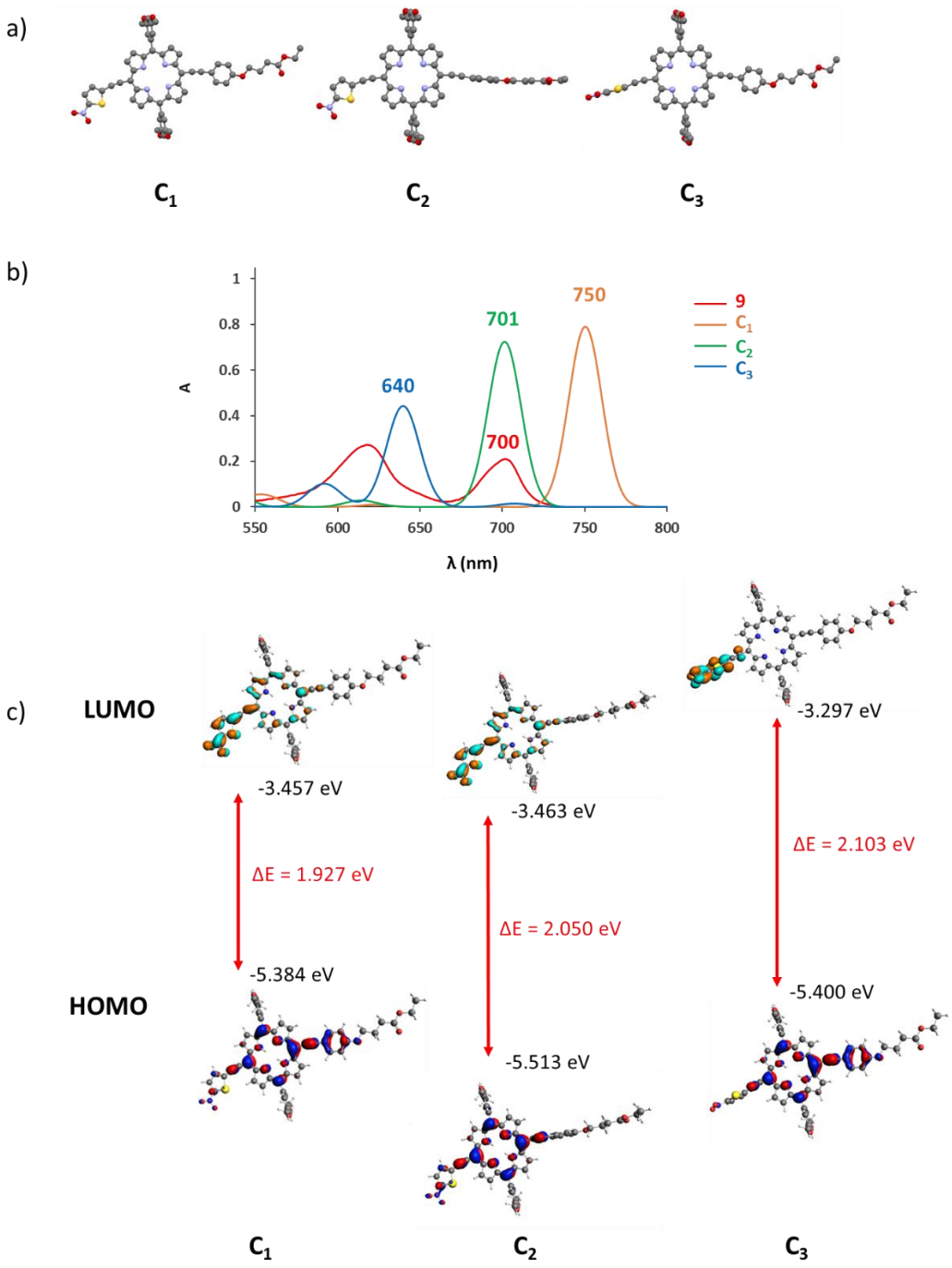

Figure 2. (a) Optimized geometry of the conformers **C1-C3** and (b) lowest computed absorption bands of **C1-C3** and experimental spectra of **9** in DCM. (c) Calculated frontier molecular orbitals and associated energy levels of the structures **C1-C3**.

Antimicrobial assays

Photoinactivation of Gram-negative bacteria

Gram-negative bacteria are endowed with cell envelopes of low permeability to chemicals consisting of a triple layer of plasma membrane, cell wall and outer membrane which make them difficult to kill. *Escherichia coli* (*E. coli*) is not only ubiquitous in animals and humans but also some strains of this species belong to the ESKAPE pathogens, being dangerous to human health and multiresistant to the most common treatments. Therefore *E. coli* laboratory strains are often used as model of Gram-negative bacteria to track emerging resistance,[54] and were also selected in this work to test the photobactericidal activity of the designed conjugate **1**. As shown in Figure 3, *E. coli* incubated with 1 µM of compound **1** and subjected to 15 min irradiation at 720 nm gave a 3 $\log_{10}$ reduction in bacterial viability. Thus, this low concentration corresponds to the minimum bactericidal concentration (MBC) where ≥ 99.9% of the bacteria are killed. Increasing the incubation concentration to 2.5 µM lead to 3.7 $\log_{10}$ of cell death and at a concentration of 5 µM, a 4.5 $\log_{10}$ reduction in cell viability was obtained. In the dark, a low antimicrobial effect of 8 to 22 % was observed for the conjugate **1** at these concentrations. At the highest concentration tested, 5 µM of the **PGLa** or the photosensitizer **9** alone resulted in the killing of 13% and 4% of the bacteria, respectively (see SI Table S2). The antibacterial activity of **PGLa** and **9** did not increase upon excitation at 720 nm demonstrating the synergistic effect of the PS and targeting-peptide constituents of **1** with that of light, to kill these bacteria.

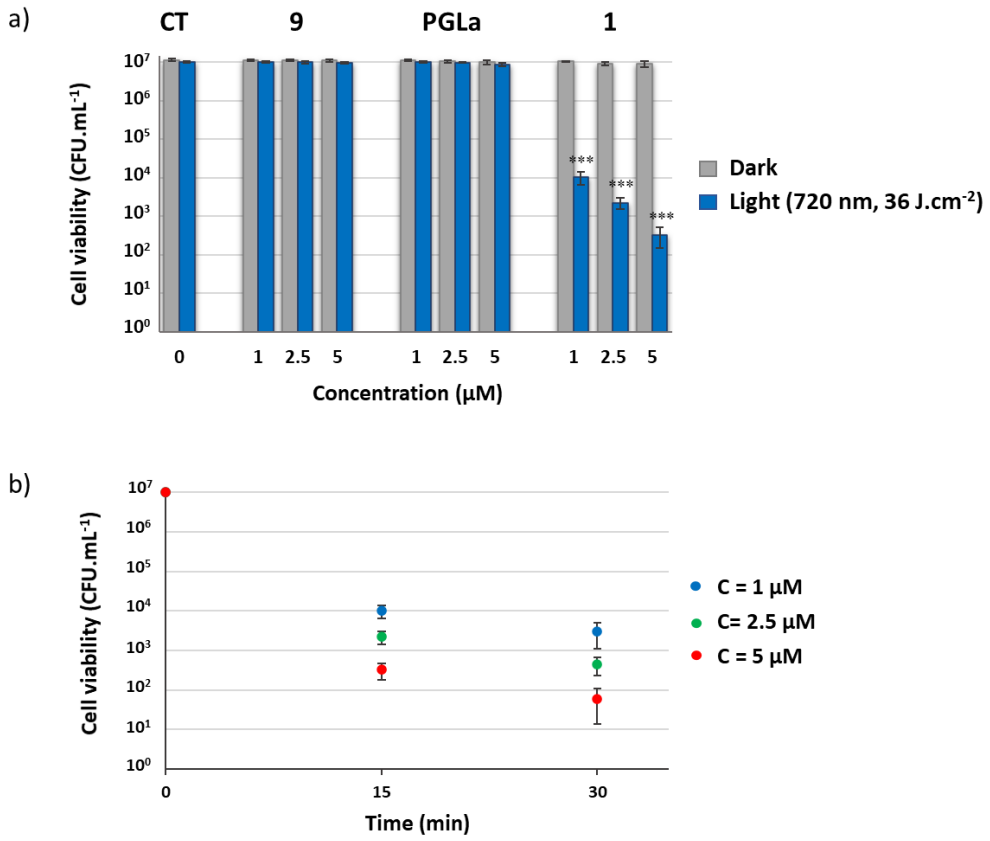

Figure 3. (a) Cell viability of *E. coli* incubated 15 min with **9**, **PGLa** or conjugate **1** at different concentrations followed by 15 min incubation with light irradiation (at 720 nm, LED power 40 $mW.cm^{-2}$) or in the dark. CT: control, survival fraction without conjugate. (b) Effect of the irradiation time of the conjugate **1** on *E. coli* survival. Data are representative of at least three independent experiments and values are expressed in mean ± SE. ***$p < 0.001$ significance compared to control; data without symbols are not significantly different $p > 0.05$. p-values were determined by unpaired *t* tests.

Effect of the irradiation time

To test the effect of irradiation time on the photobactericidal activity, the time of exposure to light was increased from 15 to 30 min keeping the fluence rate at 40 $mW.cm^{-2}$. The photoinactivation increased at 1 µM from 99.91 % to 99.97% (0.5 log_{10}) and at 2.5 µM and 5 µM by 0.7 log_{10} to respectively 4.4 log_{10} and 5.2 log_{10} of *E. coli* killing (Figure 3b). Increased

uptake over time of **1** by bacteria (as evidenced by absorption measurements, see below) and an increase in their probability to be excited with longer light exposure may account for these results. Nevertheless, at the concentrations tested, prolonging the irradiation by 15 min has a moderate impact when compared to the first 15 min. To check if photobleaching of the photosensitizer could limit the activity of the conjugate over time, the absorption of **1** in 150 mM PBS solution was measured after 15 and 30 min of light excitation. Limited degradation of the compound was evidenced with a decrease of the absorbance at the maximal wavelength by 12 % and 16 % at 36 $J.cm^{-2}$ and 72 $J.cm^{-2}$, respectively (see SI, Figure S36).

Regarding the antimicrobial activity of the conjugate in the dark, it slightly increased from 15 to 30 min but remained below 30% (see Table S2-S3). For the PS and PGLa alone, the activity in the dark did not increase with incubation time.

Photoinactivation of Gram-positive bacteria

Staphylococcus aureus (S. *aureus*) is a Gram-positive bacterium prone to produce high virulence factors and a main source of serious infections in hospitals.[55]

The conjugate **1** was tested on *S. aureus* in the same conditions as for *E. coli*. The MBC was reached at a low concentration of 1 µM with 3.2 $\log_{10}$ of cell death after 15 min of irradiation (Figure 4). This result is comparable to the one observed on *E. coli* and might be related, at this low concentration, to the strong targeting ability of the conjugate against both types of bacteria. By increasing the incubation concentration, the photoinactivation effect was much more pronounced as compared to the effect on *E. coli* with 5.7 $\log_{10}$ of killing at 2.5 µM and a complete eradication reached at 5 µM concentration (7 $\log_{10}$). This stronger effect towards *S. aureus* may be related to their membranes which are easier to destabilize and thus more sensitive to the cooperative effect of the membrane-targeting conjugate and the ROS generated on the membrane following light irradiation.

The dark antimicrobial efficiency observed for **1** was higher than the one observed against *E. coli* (24-65% at the range of concentrations used, Table S4) and the same was observed for the antimicrobial peptide **PGLa** alone (11-40 % dark antimicrobial effect) in accordance with greater accessibility of the *S. aureus* cytoplasmic membrane. The porphyrin alone **9** displayed low activity with less than 7 % of bacteria killed at the highest concentration. Under illumination, the antibacterial effect of **9** or **PGLa** on *S. aureus* did not increase significantly as compared to the conjugate suggesting that **9** has a lower accessibility to and/or affinity for membranes (Figure 4).

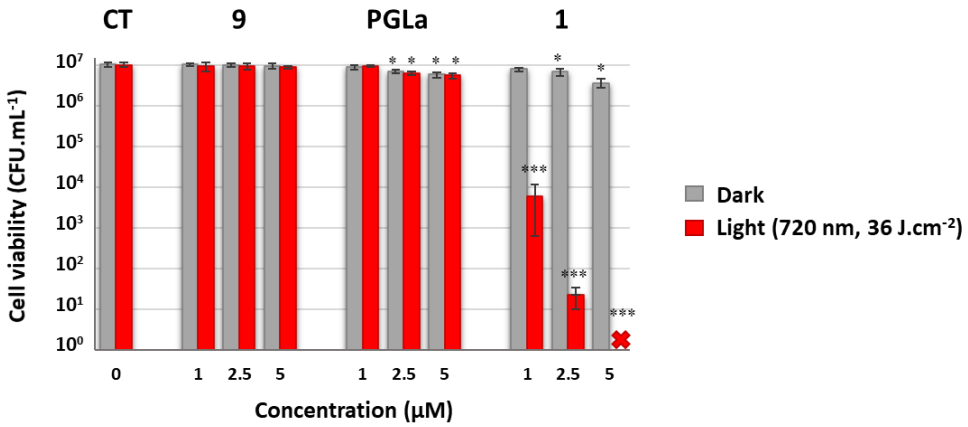

Figure 4. Cell viability of *S. aureus* incubated 15 min with **9**, **PGLa** or conjugate **1** at different concentrations followed by 15 min incubation with light irradiation (720 nm, LED power 40 $mW.cm^{-2}$) or in the dark. CT: control, survival fraction without conjugate. The cross corresponds to a complete photoeradication (7 log_{10} units reduction). Data are representative of at least three independent experiments and values are expressed in mean ± SE. *$p < 0.05$, ***$p < 0.001$ significance compared to control; data without symbols are not significantly different $p > 0.05$. p-values were determined by unpaired *t* tests.

Toxicity for eukaryotic cells

Normal human epidermal keratinocytes (NHEK) cells involved in healing skin infections were used to assess the toxicity of the conjugate. Dark toxicity and phototoxicity were evaluated in

the same conditions used for bacteria, 15 min of irradiation at 720 nm (fluence 36 J.cm^{-2}) with the conjugate **1** or one of its building blocks alone, i.e. **9** and **PGLa**. The cell viability was evaluated using an XTT test.

No dark toxicity was observed for the conjugate **1** at 1 µM and a moderate toxicity of 15 % and 23% was obtained at 2.5 and 5 µM respectively, whereas **9** and **PGLa** alone did not reach 10% of toxicity at all concentration studied (Figure 5). These results demonstrate that **PGLa** alone or linked to the photosensitizer has low ability to target these skin cells.

Regarding the photoinactivation of the NHEK no additional phototoxicity of **9** or **PGLa** alone compared to the dark toxicity was detected even at 5 µM in agreement with their low affinity for this cell line. Very promising is the negligible phototoxicity of 4.5 % of the conjugate **1** incubated at 1 µM with light irradiation (Figure 5). The phototoxicity increased with the concentration with 50 % and 81% of cell death detected at 2.5 µM and 5 µM, respectively. Therefore, in view of the results obtained on bacteria, selective and efficient a-PDT treatment with near IR light can be performed at a low 1 µM incubation concentration.

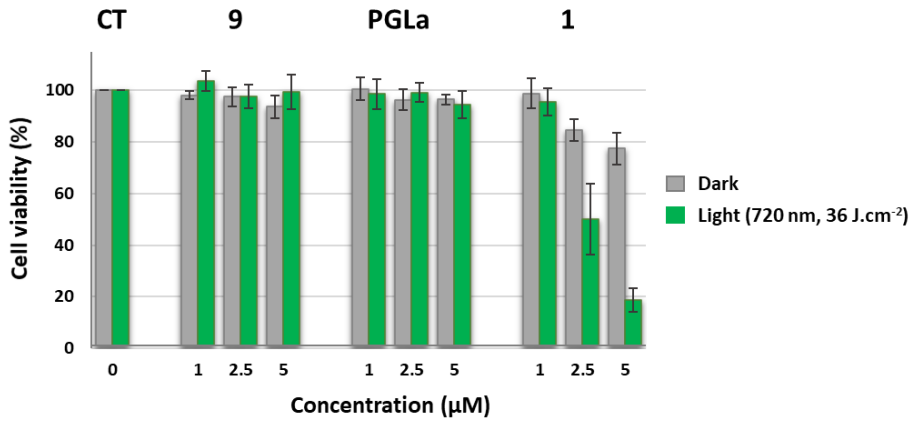

Figure 5. Toxicity and phototoxicity (720 nm, 15 min irradiation) of **1**, **PGLa** and **9**, evaluated on NHEK cells. Data are representative of at least three independent experiments and values are expressed in mean ± SE.

Photobactericidal effect of the conjugate with white light

To compare the photobactericidal effect with visible light on *E. coli* under the same incubation conditions, the bacteria were irradiated with white LED (400-700 nm, 40 mW.cm^{-2}) for 15 min, to reach an equivalent light dose of 36 J.cm^{-2}. The photosensitizer **9** and the antimicrobial peptide **PGLa** showed weak photoinactivation of bacteria comparable to that obtained with 720 nm irradiation (Figure 6). The photoinactivation observed at 1 µM concentration for **1** with white light was more pronounced than with red light, with 3.9 $\log_{10}$ reduction and 4.6 $\log_{10}$ at 2.5 µM. At 5µM, a total eradication of the bacteria was observed under these irradiation conditions. With the wide illumination range of white light, both intense absorption bands at 453 nm and 653 nm of **1** in PBS can contribute to the excitation of the photosensitizer thus enhancing the photoinactivation effect.

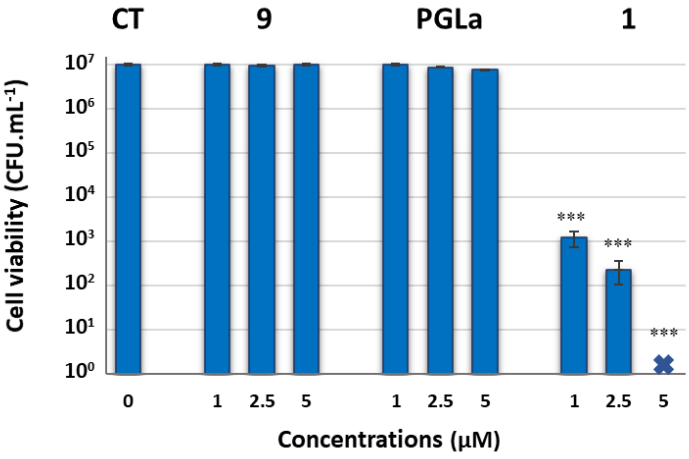

Figure 6. Survival of *E. coli* incubated for 15 min with **9**, **PGLa** or conjugate **1** at different concentrations followed by 15 min incubation with white light irradiation (LED power 40 mW.cm^{-2}). CT: control, survival fraction without conjugate. The cross corresponds to a complete photoeradication (7 $\log_{10}$ units reduction). Data are representative of at least three independent experiments and values are expressed in mean ± SE. ***$p < 0.001$ significance compared to control; data without symbols are not significantly different $p > 0.05$. p-values were determined by unpaired *t* tests.

Association of the conjugate by bacteria

To estimate the affinity of the conjugate for bacterial membranes, UV-vis absorption spectroscopy was used to assess the amount of conjugate remaining in the supernatant solution after incubation of *E. coli* in PBS. For such, **1** at a concentration of 5 µM was incubated for 15 or 60 min with *E. coli* at 10^8 CFU.mL^{-1} in PBS. After centrifugation of the medium, the supernatant was collected and the absorbance measured compared to the one of the solution of the conjugate at 5 µM in PBS in absence of bacteria. The data obtained revealed a significant association of **1** by bacteria of 45% following 15 min of incubation that increased to 76% for one hour of incubation (see Figure S37).

The binding of the conjugate to *E. coli* one hour after incubation was confirmed by confocal fluorescence microscopy. The image obtained following excitation at 458 nm shows the fluorescence of **1** bound to the bacteria (Figure 7). All bacteria observed are labelled in red indicating that the compound **1** is effective to target membranes. Moreover, to confirm that **1** is located on bacterial membranes, we performed super-resolution confocal images (Figure 7c). Bacteria cytoplasms were labelled with a DAPI dye (blue) that targets DNA and we clearly observed that red fluorescence from **1** is localized all around the membrane and not intracellularly. As detailed in Figure S38, no colocalization of red and blue fluorescences is observed on images of different bacteria.

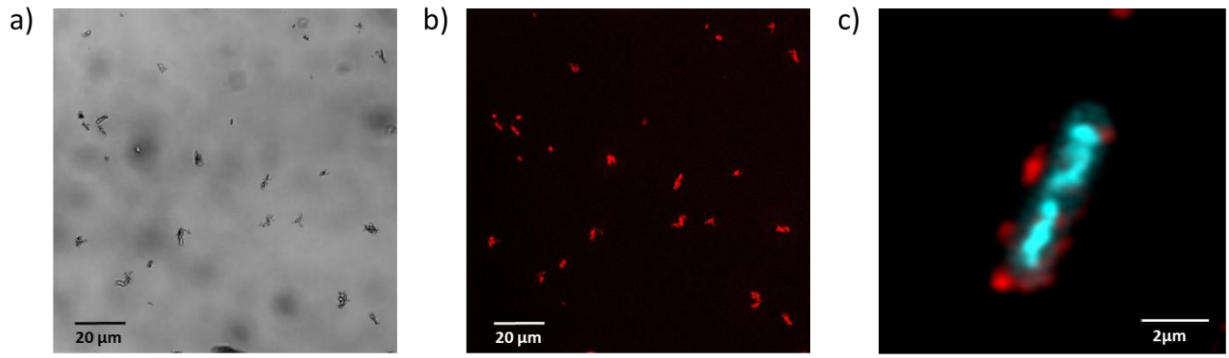

Figure 7. Confocal microscopy images of *E. coli* incubated with **1** at 5 µM for 1h in PBS buffer. (a) Bright field image, (b) confocal microscopy image, with **1** in red fluorescence (λ_{exc} = 458 nm, λ_{em} = 653-740 nm), and (c) super-resolution confocal microscopy (Airy scan detector, Zeiss) with **1** in red fluorescence (λ_{exc} = 458 nm, λ_{em} = 653-740 nm) and bacteria cytoplasm with DNA labelled with DAPI (blue fluorescence, λ_{exc} = 405 nm, λ_{em} = 400-479 nm).

CONCLUSION

The design of an extended π-conjugated photosensitizer linked to an antimicrobial peptide enabled its excitation in the near IR to perform a-PDT in the optical therapeutic window. The conjugate has shown good photostability and capacity to generate singlet oxygen. Its ability to associate to the bacteria was shown by its fluorescence on *E. coli* cells. In the absence of light, the conjugate has no or low capacity to kill bacteria or keratinocytes in the concentration range of 1-5 µM. On the other hand, strong photobactericidal effects were obtained on both Gram-positive *S. aureus* and Gram-negative *E. coli* bacteria with already 3 $\log_{10}$ reduction of survival when incubated at a low 1 µM concentration upon irradiation at 720 nm for 15 min. The photoinactivation activity increased to 4.5 $\log_{10}$ at 5 µM on *E. coli* and at this incubation concentration, a complete eradication of *S. aureus* was achieved. These results underline the synergistic effect of the designed molecular association with that of light for photodynamic disinfection. Moreover, the antimicrobial **PGLa** peptide of the conjugate provides a selective

targeting of bacteria when compared to keratinocytes thus at 1 µM, under near IR light irradiation, the MBC is reached for bacteria without phototoxicity to human cells. In these conditions, neither the constituents alone, **PGLa** and PS, nor the light alone damage the bacteria. Thus, the molecular conjugate shows strong potential as antibacterial agent for the safe treatment of infections and deep wounds with low light energy.

METHODS

Standard methods are described in the Supporting Information.

Synthesis

Porphyrin-peptide conjugate 1. To a solution of porphyrin **2** (11 mg, 7.48 µmol, 1 equiv) in DMF (1 mL) was added TBTU (7.2 mg, 22.4 µmol, 3 equiv) and DIPEA (13 µL, 75 µmol, 10 equiv). The reaction mixture was stirred at room temperature for 1 hour. In parallel, resin-grafted PGLa **3** (285 mg, 37.1 µmol, 5 equiv) was swelled in DMF for 1 h. The solution of porphyrin, TBTU and DIPEA were then added to **3** and the reaction mixture was gently stirred for 72 h. After filtration, the grafted resin was washed with DMF (2 x 5 mL). Cleavage and deprotection were performed using 5 mL of a solution of HFIP/TFA (99 : 1) for 2 h at room temperature. Then the resin was filtrated and washed with HFIP (3 x 2 mL) and the filtrate was poured into diethyl ether and centrifuged three times. The resulting solid was dissolved in H_2O and lyophilized. The crude product was purified by reverse-phase HPLC (H_2O/MeCN 90 : 10 with 0.1 % TFA / MeCN with 0.1 % TFA, with a linear gradient from 45/55 to 20/80 in 25 min) and the fractions containing the pure compound were lyophilized to lead to the conjugate **1** as a green TFA salt in 40 % yield (11.6 mg). **HPLC t_R** = 20.76 min **HR ESI-MS:** *m/z* 1143.9333 $[M + 3\ H]^{3+}/3$, (calcd 1143.9303 for $[C_{166}H_{252}N_{31}O_{43}S]^{3+}/3$). **UV-Visible** (DMSO): λ_{max}(nm) (log ε) = 459 (5.26), 619 (4.67), 702 (4.58) nm. **UV-Visible** (PBS): λ_{max} (log ε) = 455 (4.74),

636 (4.34), 720 (4.32) nm.

Light Sources

LED irradiation was achieved using 720 nm LEDs purchased from Shenzhen Litlight Electronic Co. which were then mounted on aluminium heat sinks to give a homemade irradiation setup. The peak emission wavelength of LEDs is matched with the lowest (energy) absorption band of the conjugate. The setup was placed on the top of the 96-well plate and the light irradiance was measured to be 40 $mW.cm^{-2}$ by a Thorlabs PM100D powermeter.

White light irradiation was performed using white light LEDs (400-700 nm wavelength range) purchased from Future Eden Ltd, which were then mounted on aluminium heat sinks to give a homemade irradiation setup. The ISO-TECH LUX-1335 digital light meter was used to precisely measure the light intensity.

Bacterial cultures. *S. aureus* CIP76.25 were obtained from Institut Pasteur (Paris, France). These strains were cultured in liquid tryptic soy (pancreatic casein extract, 17 $g.L^{-1}$; soy flour papaic digest, 3 $g.L^{-1}$; dextrose, 2.5 $g.L^{-1}$; NaCl, 5 $g.L^{-1}$; and K_2HPO_4, 2.5 $g.L^{-1}$) and incubated overnight at 37 °C under aerobic conditions.

E. coli ATCC25922 were obtained from Thermo Fisher Scientific (Courtaboeuf, France). These strains were cultured in liquid Mueller-Hinton (beef infusion solids, 2 $g.L^{-1}$; starch, 1.5 $g.L^{-1}$; casein hydrolysate, 17.5 $g.L^{-1}$) and incubated overnight at 37 °C under aerobic conditions.

Bacterial photoinactivation. Bacteria were grown overnight in MH medium at 37 °C, harvested by centrifugation (3200 g, 5 min), washed twice with PBS 1X (3200 g, 5 min) and resuspended in PBS 1X at a density of 2.10^7 $CFU.mL^{-1}$. The bacterial concentration in stationary phase was estimated by reading the turbidity of the suspension at 550 nm in a

Multiskan Go ThermoFisher Scientific spectrophotometer. The peptide **PGLa** and the conjugate **1** were solubilized in PBS 1X at different concentrations. The neutral porphyrin **9** was solubilized in DMSO then in PBS 1X at different concentrations (final DMSO concentration never exceeded 0.5 %). The bacteria were transferred into a 96-well plate (Thermo Scientific Nunc®) for a final cell density of 10^7 CFU.mL^{-1} (200 µL/well) and then incubated in the dark at 37 °C for 15 min with different concentrations of the compounds. The wells containing bacteria and compounds were irradiated for 15 min with near IR light (720 nm, 40 mW.cm^{-2} for a fluence of 36 J.cm^{-2}) or white light (36 J.cm^{-2}) with a homemade apparatus placed above the 96-well plate. As controls without irradiation, plates were kept in the dark at room temperature. Bacterial content of each well was taken and then serially diluted in PBS and 100 µL of appropriate diluted samples were spread on MH agar plates. For the most photoactive compounds, bacterial content of the well was directly spread on MH agar plates without dilution. After incubation overnight at 37 °C, colonies were counted to determine total CFU.mL^{-1}. The survival rate was calculated by comparing the bacterial concentrations of the treated wells with the initial concentration obtained from controls. Controls included bacteria without compounds in the dark, irradiated and in the presence of 0.5 % of DMSO.
Each experiment was performed three times with independent bacterial suspensions.

***E. coli* association experiments.** *E. coli* cells at a density of 10^8 CFU.mL^{-1} were incubated with **1** at a concentration of 5 µM in PBS 1X at 37 °C for 15 min or 60 min in the dark (total volume of each sample was 400 µL in 1 mL tube). After centrifugation of the tubes (3200 g, 5 min), 100 µL of supernatant was transferred to a spectrophotometer cuvette. The absorption was measured with a Multiskan Go ThermoFisher Scientific spectrophotometer. Control samples without bacteria were treated the same and their absorbance values represented the value of reference. All conditions and controls were measured in triplicate.

Confocal microscopy. Confocal images were acquired on a confocal laser scanning miscroscope Zeiss 710 using a x63 oil Plan Apo (NA 1.4) objective and an argon laser (458 nm) to excite the conjugate. Emitted fluorescence was monitored between 653 and 740 nm. Image acquisition and analysis were realized with a Zeiss ZEN software (ZEN 2.3 SPI).

For high-resolution confocal images, a specific sample preparation was followed. Suspension of *E. coli* in PBS (2.10^7 UFC.mL^{-1}) was incubated with 5 µM of conjugate **1** during 15 min in the dark at 37°C. Then, the bacterial suspension was deposited for 15 min on a 12 mm diameter glass slide in a 24 wells plate. The supernatant was removed and then adhering bacteria were fixed with PFA (paraformaldehyde, Sigma, France) during 15 min and washed with PBS twice. DNA was labelled with DAPI (4',6-diamidino-2-phénylindole, 1µg.mL^{-1}, Invitrogen France). After two washes, the samples were mounted with VectaShield (Vectore Laboratories, USA). High resolution images of bacteria were acquired using an inverted LSM 800 confocal scanning microscope with Airyscan detector (Zeiss, Germany) using a 63x Plan Apo (N.A. 1.4, oil immersion objective). The Zen Blue software from Zeiss was used for image capture. DAPI fluorochrome was detected between 400 and 479 nm after excitation at λ = 405 nm and **1** was detected between 653 and 740 nm after excitation at 458 nm.

Keratinocytes (NHEK) cultures. The human normal keratinocyte cell line NHEK (NHEK-Adult KGM-Gold, Lonza) was cultured in keratinocyte basal medium (KBM) supplemented with a keratinocyte growth medium-2 (KBM-2) Bullet kit (Lonza). NHEK cells were cultured at 37 °C in 95 % humified air in the presence of 5 % CO_2.

Cytotoxicity and phototoxicity on keratinocytes. Keratinocytes in KBM culture medium were seeded in a 96-well plate (Thermo Scientific Nunc) 24 h prior to the tests (100 µL, 10^4

cell suspension per well). The peptide **PGLa** and the conjugate **1** were solubilized in PBS 1X at different concentrations. The neutral porphyrin **9** was solubilized in DMSO then in PBS 1X at different concentrations (final DMSO concentration never exceeded 0.5 %). Culture medium was removed and cells were incubated 15 min in the dark with the compounds. The wells were irradiated for 15 min with near IR light (720 nm, 40 $mW.cm^{-2}$, fluence of 36 J. cm^{-2}) with a homemade apparatus placed above the 96-well plate. As controls without irradiation, plates were kept in the dark at room temperature. Then, PBS was removed and 150 µL of fresh KBM culture medium was added in the wells. The plates were placed in the incubator at 37 °C and cell viability was determined using the tetrazolium salt 2,3-bis-(2-methoxy-4-nitro-5-sulfophenyl)-2H-tetrazolium-5-carboxanilide) (XTT) test. After 24h at 37 °C, the solution of XTT and PMS was added at a final concentration of 333 $\mu g.mL^{-1}$ and 2.5 $\mu g.mL^{-1}$ for XTT and PMS respectively in each well, and cells were incubated at 37 °C for 12 h. The absorbance was measured at 450 nm using a Bio-Rad iMark microplate reader. The viability of the treated cells corresponds to the ratio between the absorbance measured for the different conditions and the absorbance of untreated cells that represents 100 % viability.

Each experiment was performed three times with independent cells cultures.

Supporting Information Available

Standard methods, characterization of **2**, **3**, **5**, **6**, **8**, **9**, computational details and singlet oxygen quantum yield determinations.

Acknowledgments.

The icFRC "http://www.icfrc.fr" and LabEx CSC, are gratefully acknowledged for their support and the Ministry of Education and Research for a Ph.D. fellowship to C.G. ANR is acknowledged for the funding of the project SAFEST ANR-21-CE18-0043. GDR 2067

MAPYRO is acknowledged for financial support. Italian CNR (project PHEEL) is acknowledged.

References

(1) Website of World Health Organization (17/11/22) http://www.who.int/news-room/fact-sheets/detail/antimicrobial-resistance.

(2) Agostinis, P., Berg, K., Cengel, K. A., Foster, T. H., Girotti, A. W., Gollnick, S. O., Hahn, S. M., Hamblin, M. R., Juzeniene, A., Kessel, D., Korbelik, M., Moan, J., Mroz, P., Nowis, D., Piette, J., Wilson, B. C., Golab, J. (2011) Photodynamic Therapy of Cancer: An Update. *CA: Cancer J. Clin. 61*, 250–281. https://doi.org/10.3322/caac.20114.

(3) Pham, T. C., Nguyen V.-N., Choi, Y., Lee, S., Yoon, J. (2021) Recent Strategies to Develop Innovative Photosensitizers for Enhanced Photodynamic Therapy. *Chem. Rev. 121*, 13454–13619. https://doi.org/10.1021/acs.chemrev.1c00381

(4) Hamblin, M. R., Hasan, T. (2004) Photodynamic Therapy: A New Antimicrobial Approach to Infectious Disease? *Photochem. Photobiol. Sci. 3*, 436–450. https://doi.org/10.1039/b311900a.

(5) Anas, A., Sobhanan, J., Sulfiya, K. M., Jasmin, C., Sreelakshmi, P. K., Biju, V. (2021) Advances in photodynamic antimicrobial chemotherapy, *J. Photochem. Photobiol. C: Photochem. Rev. 49*, 100452. https://doi.org/10.1016/j.jphotochemrev.2021.100452

(6) Maisch, T. (2015) Resistance in Antimicrobial Photodynamic Inactivation of Bacteria. *Photochem. Photobiol. Sci. 14*, 1518–1526. https://doi.org/10.1039/C5PP00037H.

(7) Maldonado-Carmona, N., Ouk, T.-S., Leroy-Lhez, S. (2021) Latest Trends on Photodynamic Disinfection of Gram-Negative Bacteria: Photosensitizer's Structure and

Delivery Systems. *Photochem. Photobiol. Sci.* 21, 113–145. https://doi.org/10.1007/s43630-021-00128-5.

(8) Tanaka, M., Mroz, P., Dai, T., Huang, L., Morimoto, Y., Kinoshita, M., Yoshihara, Y., Nemoto, K., Shinomiya, N., Seki, S., Hamblin, M. R. (2012) Photodynamic Therapy Can Induce a Protective Innate Immune Response against Murine Bacterial Arthritis via Neutrophil Accumulation. *PLoS ONE 7*, e39823. https://doi.org/10.1371/journal.pone.0039823.

(9) George, S., Hamblin, M. R., Kishen, A. (2009) Uptake Pathways of Anionic and Cationic Photosensitizers into Bacteria. *Photochem. Photobiol. Sci. 8*, 788–795. https://doi.org/10.1039/b809624d.

(10) Morales-de-Echegaray, A. V., Maltais, T. R., Lin, L., Younis, W., Kadasala, N. R., Seleem, M. N., Wei, A. (2018) Rapid Uptake and Photodynamic Inactivation of Staphylococci by Ga(III)-Protoporphyrin IX. *ACS Infect. Dis. 4*, 1564–1573. https://doi.org/10.1021/acsinfecdis.8b00125

(11) Jiang, L., Gan, C. R. R., Gao, J., Loh, X. J. (2016) A Perspective on the Trends and Challenges Facing Porphyrin-Based Anti-Microbial Materials. *Small 12*, 3609–3644. https://doi.org/10.1002/smll.201600327.

(12) Alenezi, K., Tovmasyan, A., Batinic-Haberle, I., Benov, L. T. (2017) Optimizing Zn Porphyrin-Based Photosensitizers for Efficient Antibacterial Photodynamic Therapy. *Photodiagnosis Photodyn. Ther. 17*, 154–159. https://doi.org/10.1016/j.pdpdt.2016.11.009.

(13) Vinagreiro, C. S., Zangirolami, A., Schaberle, F. A., Nunes, S. C. C., Blanco, K. C., Inada, N. M., da Silva, G. J., Pais, A. A. C. C., Bagnato, V. S., Arnaut, L. G., Pereira, M. M. (2020) Antibacterial Photodynamic Inactivation of Antibiotic-Resistant Bacteria and

Biofilms with Nanomolar Photosensitizer Concentrations. *ACS Infect. Dis. 6*, 1517–1526. https://doi.org/10.1021/acsinfecdis.9b00379.

(14) Le Guern, F., Ouk, T.-S., Yerzhan, I., Nurlykyz, Y., Arnoux, P., Frochot, C., Leroy-Lhez, S., Sol, V., (2021) Photophysical and Bactericidal Properties of Pyridinium and Imidazolium Porphyrins for Photodynamic Antimicrobial Chemotherapy. *Molecules* 26, 1122–1142. https://doi.org/10.3390/molecules26041122

(15) Tegos, G. P., Masago, K., Aziz, F., Higginbotham, A., Stermitz, F. R., Hamblin, M. R. (2008) Inhibitors of Bacterial Multidrug Efflux Pumps Potentiate Antimicrobial Photoinactivation. *Antimicrob. Agents Chemother. 52*, 3202–3209. https://doi.org/10.1128/AAC.00006-08.

(16) Hamblin, M. R. (2002) Polycationic Photosensitizer Conjugates: Effects of Chain Length and Gram Classification on the Photodynamic Inactivation of Bacteria. *J. Antimicrob. Chemother. 49*, 941–951. https://doi.org/10.1093/jac/dkf053.

(17) Tomé, J. P. C., Neves, M. G. P. M. S., Tomé, A. C., Cavaleiro, J. A. S., Soncin, M., Magaraggia, M., Ferro, S., Jori, G. (2004) Synthesis and Antibacterial Activity of New Poly- *S* -Lysine−Porphyrin Conjugates. *J. Med. Chem. 47*, 6649–6652. https://doi.org/10.1021/jm040802v.

(18) Tegos, G. P., Anbe, M., Yang, C., Demidova, T. N., Satti, M., Mroz, P., Janjua, S., Gad, F., Hamblin, M. R. (2006) Protease-Stable Polycationic Photosensitizer Conjugates between Polyethyleneimine and Chlorin(E6) for Broad-Spectrum Antimicrobial Photoinactivation. *Antimicrob. Agents Chemother. 50*, 1402–1410. https://doi.org/10.1128/AAC.50.4.1402-1410.2006.

(19) Zasloff, M. (2019) Antimicrobial Peptides of Multicellular Organisms: My Perspective. In *Antimicrobial Peptides* (Matsuzaki, K., Ed.), *Adv. Exp. Med. Biol.* ; Springer Singapore: Singapore, Vol. 1117, pp 3–6. https://doi.org/10.1007/978-981-13-3588-4_1.

(20) Dosselli, R., Tampieri, C., Ruiz-González, R., De Munari, S., Ragàs, X., Sánchez-García, D., Agut, M., Nonell, S., Reddi, E., Gobbo, M. (2013) Synthesis, Characterization, and Photoinduced Antibacterial Activity of Porphyrin-Type Photosensitizers Conjugated to the Antimicrobial Peptide Apidaecin 1b. *J. Med. Chem. 56,* 1052–1063. https://doi.org/10.1021/jm301509n.

(21) Dosselli, R., Ruiz-González, R., Moret, F., Agnolon, V., Compagnin, C., Mognato, M., Sella, V., Agut, M., Nonell, S., Gobbo, M., Reddi, E. (2014) Synthesis, Spectroscopic, and Photophysical Characterization and Photosensitizing Activity toward Prokaryotic and Eukaryotic Cells of Porphyrin-Magainin and -Buforin Conjugates. *J. Med. Chem. 57*, 1403–1415. https://doi.org/10.1021/jm401653r.

(22) Bourré, L., Giuntini, F., Eggleston, I. M., Mosse, C. A., MacRobert, A. J., Wilson, M. (2010) Effective Photoinactivation of Gram-Positive and Gram-Negative Bacterial Strains Using an HIV-1 Tat Peptide–Porphyrin Conjugate. *Photochem. Photobiol. Sci. 9*, 1613–1620. https://doi.org/10.1039/c0pp00146e.

(23) Zhang, A.-N., Wu, W., Zhang, C., Wang, Q.-Y., Zhuang, Z.-N., Cheng, H., Zhang, X.-Z. (2019) A Versatile Bacterial Membrane-Binding Chimeric Peptide with Enhanced Photodynamic Antimicrobial Activity. *J. Mater. Chem. B* 2 7, 1087–1095. https://doi.org/10.1039/C8TB03094D.

(24) Yang, W., Yoon, Y., Lee, Y., Oh, H., Choi, J., Shin, S., Lee, S., Lee, H., Lee, Y., Seo, J. (2021) Photosensitizer–Peptoid Conjugates for Photoinactivation of Gram-Negative Bacteria: Structure–Activity Relationship and Mechanistic Studies. *Org. Biomol. Chem. 19*, 6546–6557. https://doi.org/10.1039/D1OB00926E.

(25) Le Guern, F., Sol, V., Ouk, C., Arnoux, P., Frochot, C., Ouk, T.-S. (2017) Enhanced Photobactericidal and Targeting Properties of a Cationic Porphyrin Following the

Attachment of Polymyxin B. *Bioconjugate Chem. 28*, 2493–2506. https://doi.org/10.1021/acs.bioconjchem.7b00516.

(26) Le Guern, F., Ouk, T.-S., Ouk, C., Vanderesse, R., Champavier, Y., Pinault, E., Sol, V. (2018) Lysine Analogue of Polymyxin B as a Significant Opportunity for Photodynamic Antimicrobial Chemotherapy. *ACS Med. Chem. Lett. 9*, 11–16. https://doi.org/10.1021/acsmedchemlett.7b00360.

(27) Ucuncu, M., Mills, B., Duncan, S., Staderini, M., Dhaliwal, K., Bradley, M. (2020) Polymyxin-Base Photosensitizer for the Potent and Selective Killing of Gram-Negative Bacteria *Chem. Commun. 56*, 3757–3760. https://doi.org/10.1039/C7CC08099A.

(28) Bayat, F., Karimi, A. R. (2019) Design of Photodynamic Chitosan Hydrogels Bearing Phthalocyanine-Colistin Conjugate as an Antibacterial Agent. *Int. J. Biol. Macromol. 129*, 927–935. https://doi.org/10.1016/j.ijbiomac.2019.02.081.

(29) Liu, F., Soh Yan Ni, A., Lim, Y., Mohanram, H., Bhattacharjya, S., Xing, B. (2012) Lipopolysaccharide Neutralizing Peptide–Porphyrin Conjugates for Effective Photoinactivation and Intracellular Imaging of Gram-Negative Bacteria Strains. *Bioconjugate Chem. 23*, 1639–1647. https://doi.org/10.1021/bc300203d.

(30) Ethirajan, M., Chen, Y., Joshi, P., Pandey, R. K. (2011) The Role of Porphyrin Chemistry in Tumor Imaging and Photodynamic Therapy. *Chem. Soc. Rev. 40*, 340–362. https://doi.org/10.1039/B915149B.

(31) Finlayson, L., Barnard, I. R. M., McMillan, L., Ibbotson, S. H., Brown, C. T. A., Eadie, E., Wood, K. (2021) Depth Penetration of Light into Skin as a Function of Wavelength from 200 to 1000 nm. *Photochem. Photobiol.* https://doi.org/10.1039/B915149B.

(32) Ash, C., Dubec, M., Donne, K., Bashford, T. (2017) Effect of wavelength and beam width on penetration in light-tissue interaction using computational methods. *Lasers Med. Sci. 32*, 1909–1918. https://doi.org/10.1007/s10103-017-2317-4.

(33) Aroso, R. T., Schaberle, F. A., Arnaut, L. G., Pereira, M. M. (2021) Photodynamic disinfection and its role in controlling infectious diseases. *Photochem Photobiol Sci 20*, 1497–1545. https://doi.org/10.1007/s43630-021-00102-1.

(34) Huang, L., Krayer, M., Roubil, J. G. S., Huang, Y.-Y., Holten, D., Lindsey, J. S., Hamblin, M. R. (2014) Stable Synthetic Mono-Substituted Cationic Bacteriochlorins Mediate Selective Broad-Spectrum Photoinactivation of Drug-Resistant Pathogens at Nanomolar Concentrations. *J. Photochem. Photobiol. B 141*, 119–127. https://doi.org/10.1016/j.jphotobiol.2014.09.016.

(35) Vecchio, D., Dai, T., Huang, L., Fantetti, L., Roncucci, G., Hamblin, M. R. (2013) Antimicrobial Photodynamic Therapy with RLP068 Kills Methicillin-Resistant *Staphylococcus Aureus* and Improves Wound Healing in a Mouse Model of Infected Skin Abrasion PDT with RLP068/Cl in Infected Mouse Skin Abrasion. *J. Biophoton. 6,* 733–742. https://doi.org/10.1002/jbio.201200121.

(36) Giuliani, F., Martinelli, M., Cocchi, A., Arbia, D., Fantetti, L., Roncucci, G. (2010) *In Vitro* Resistance Selection Studies of RLP068/Cl, a New Zn(II) Phthalocyanine Suitable for Antimicrobial Photodynamic Therapy. *Antimicrob. Agents Chemother. 54*, 637–642. https://doi.org/10.1128/AAC.00603-09.

(37) Galstyan A., Schiller R., Dobrindt U. (2017) Boronic Acid Functionalized Photosensitizers: A Strategy To Target the Surface of Bacteria and Implement Active Agents in Polymer Coatings. *Angew. Chem. Int. Ed. Engl. 21*, 10362–10366. https://doi.org/10.1002/anie.201703398.

(38) Andreu, D., Aschauer, H., Kreil, G., Merrifield, R. B. (1985) Solid-Phase Synthesis of PYLa and Isolation of Its Natural Counterpart, PGLa [PYLa-(4-24)] from Skin Secretion of Xenopus Laevis. *Eur. J. Biochem. 149*, 531–535. https://doi.org/10.1111/j.1432-1033.1985.tb08957.x.

(39) Lohner, K., Prossnigg, F. (2009) Biological Activity and Structural Aspects of PGLa Interaction with Membrane Mimetic Systems. *Biochimica et Biophysica Acta (BBA) - Biomembranes 1788*, 1656–1666. https://doi.org/10.1016/j.bbamem.2009.05.012.

(40) Bechinger, B. (1999) The Structure, Dynamics and Orientation of Antimicrobial Peptides in Membranes by Multidimensional Solid-State NMR Spectroscopy. *Biochim. Biophys. Acta Biomembr. 1462*, 157–183. https://doi.org/10.1016/S0005-2736(99)00205-9.

(41) Gautier, R., Douguet, D., Antonny, B., Drin, G. (2008) HELIQUEST: a web server to screen sequences with specific alpha-helical properties. *Bioinformatics. 24*, 2101–2102. https://doi.org/ 10.1093/bioinformatics/btn392.

(42) Bechinger, B., Zasloff, M., Opella, S. J. (1998) Structure and Dynamics of the Antibiotic Peptide PGLa in Membranes by Solution and Solid-State Nuclear Magnetic Resonance Spectroscopy *Biophys. J. 74*, 981–987. https://doi.org/10.1016/S0006-3495(98)74021-4.

(43) Jindal, M. H., Le, C. F., Mohd Yusof M. Y., Sekaran S. D. (2014) Net charge, hydrophobicity and specific amino acids contribute to the activity of antimicrobial peptides *J. Univ. Malaya Med. Cent.*, 1–7. https://doi.org/ 10.22452/jummec.vol17no1.1

(44) Aisenbrey, C., Marquette, A., Bechinger, B. (2019) The Mechanisms of Action of Cationic Antimicrobial Peptides Refined by Novel Concepts from Biophysical Investigations. In *Antimicrobial Peptides* (Matsuzaki, K., Ed.), *Adv. Exp. Med. Biol.*; Springer Singapore: Singapore ; Vol. 1117, pp 33–64. https://doi.org/10.1007/978-981-13-3588-4_4.

(45) Bechinger, B. (2015) The SMART Model: Soft Membranes Adapt and Respond, Also Transiently, in the Presence of Antimicrobial Peptides: THE SMART MODEL FOR AMPs. *J. Pept. Sci. 21*, 346–355. https://doi.org/10.1002/psc.2729.

(46) Bechinger, B., Juhl, D. W., Glattard, E., Aisenbrey, C. (2020) Revealing the Mechanisms of Synergistic Action of Two Magainin Antimicrobial Peptides. *Front. Med. Technol. 2*, 615494. https://doi.org/10.3389/fmedt.2020.615494.

(47) Cabiscol E., Tamarit J., Ros J. (2000) Oxidative stress in bacteria and protein damage by reactive oxygen species. *Int. Microbiol.* 3, 3–8. PMID: 10963327.

(48) Aisenbrey, C., Amaro, M., Pospíšil, P., Hof, M., Bechinger, B. (2020) Highly synergistic antimicrobial activity of magainin 2 and PGLa peptides is rooted in the formation of supramolecular complexes with lipids. *Sci. Rep. 10*, 11652. https://doi.org/10.1038/s41598-020-68416-1.

(49) Schmitt, J., Heitz, V., Sour, A., Bolze, F., Ftouni, H., Nicoud, J.-F., Flamigni, L., Ventura, B. (2015) Diketopyrrolopyrrole-Porphyrin Conjugates with High Two-Photon Absorption and Singlet Oxygen Generation for Two-Photon Photodynamic Therapy. *Angew. Chem. Int. Ed. 54*, 169–173. https://doi.org/10.1002/anie.201407537.

(50) Isidro-Llobet, A., Álvarez, M., Albericio, F. (2009) Amino Acid-Protecting Groups. *Chem. Rev. 109*, 2455–2504. https://doi.org/10.1021/cr800323s.

(51) Schmitt, J., Heitz, V., Jenni, S., Sour, A., Bolze, F., Ventura, B. (2017) π-Extended Porphyrin Dimers as Efficient near-Infrared Emitters and Two-Photon Absorbers. *Supramol. Chem. 29*, 769–775. https://doi.org/10.1080/10610278.2017.1377837.

(52) Alam, Md. M., Bolze, F., Daniel, C., Flamigni, L., Gourlaouen, C., Heitz, V., Jenni, S., Schmitt, J., Sour, A., Ventura, B. (2016) π-Extended Diketopyrrolopyrrole–Porphyrin Arrays: One- and Two-Photon Photophysical Investigations and Theoretical Studies. *Phys. Chem. Chem. Phys. 18*, 21954–21965. https://doi.org/10.1039/C6CP01844K.

(53) McCormick, T. M., Bridges, C. R., Carrera, E. I., DiCarmine, P. M., Gibson, G. L., Hollinger, J., Kozycz, L. M., Seferos, D. S., (2013) Conjugated Polymers: Evaluating

DFT Methods for More Accurate Orbital Energy Modeling. *Macromolecules 46*, 3879–3886. https://doi.org/10.1021/ma4005023

(54) European Food Safety Authority EFSA J., (2008), pp. 1-4.

(55) Álvarez, A., Fernández, L., Gutiérrez, D., Iglesias, B., Rodríguez, A., García, P. (2019) Methicillin-Resistant Staphylococcus Aureus in Hospitals: Latest Trends and Treatments Base on Bacteriophages. *J. Clin. Microbiol. 57*, e01006-19. https://doi.org/10.1128/JCM.01006-19.

For Table of Contents Use Only

Antibacterial Photodynamic Therapy in the Near Infrared with a Targeting Antimicrobial Peptide Connected to a π-Extended Porphyrin.

Charly Gourlot,[§] Alexis Gosset,[§] Elise Glattard,[⊥] Christopher Aisenbrey,[⊥] Sabarinathan Rangasamy,[⊥] Morgane Rabineau,[†] Tan-Sothea Ouk,[‡] Vincent Sol,[‡] Philippe Lavalle,[†] Christophe Gourlaouen,[±] Barbara Ventura,* Burkhard Bechinger,*[⊥] and Valérie Heitz *[§]

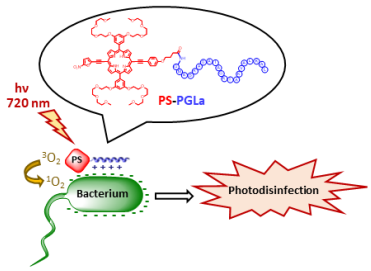

A new conjugate consisting of a PGLa antimicrobial peptide linked to a π-extended porphyrin photosensitizer shows strong bactericidal action on Gram-positive and Gram-negative bacteria upon irradiation at 720 nm.